
STOXLSTM: A STOCHASTIC EXTENDED LONG SHORT-TERM MEMORY NETWORK FOR TIME SERIES FORECASTING

Zihao Wang, Yunjie Li, Lingmin Zan, Zheng Gong

School of Information and Electronics
Beijing Institute of Technology
Beijing, China

{wangzihao24, liyunjie, zanlingmin, gongzheng}@bit.edu.cn

Mengtao Zhu ^{*}

School of Information and Electronics, Beijing Institute of Technology
Laboratory of Electromagnetic Space Cognition and Intelligent Control
Beijing, China
zhumengtao@bit.edu.cn

September 3, 2025

ABSTRACT

The Extended Long Short-Term Memory (xLSTM) network has attracted widespread research interest due to its enhanced capability to model complex temporal dependencies in diverse time series applications. Despite its success, there is still potential to further improve its representational capacity and forecasting performance, particularly on challenging real-world datasets with unknown, intricate, and hierarchical dynamics. In this work, we propose a **stochastic xLSTM**, termed **StoxLSTM**, that improves the original architecture into a state space modeling framework by incorporating stochastic latent variables within xLSTM. StoxLSTM models the latent dynamic evolution through specially designed recurrent blocks, enabling it to effectively capture the underlying temporal patterns and dependencies. Extensive experiments on publicly available benchmark datasets from multiple research communities demonstrate that StoxLSTM consistently outperforms state-of-the-art baselines with better robustness and stronger generalization ability.

Keywords Time Series Forecasting · Generative Model · xLSTM · State Space Model · Variational Inference

1 Introduction

Time series forecasting plays a vital role in numerous real-world applications, including financial market analysis [1, 2], energy systems [3, 4], weather forecasting [5], and healthcare monitoring [6]. Traditional recurrent neural networks (RNNs) [7] and their variants [8, 9], such as Long Short-Term Memory (LSTM) networks [8], have been widely used due to their capacity to model sequential data [10, 11, 12]. However, these models often struggle to capture long-range dependencies and intricate temporal structures present in many real-world time series [13].

The Extended Long Short-Term Memory network (xLSTM) [14] has emerged as a powerful architecture that enhances the conventional LSTM by introducing exponential gating mechanisms and modified memory structures. These improvements enable xLSTM to better capture complex temporal dependencies and maintain stability over long sequences. As a result, xLSTM has demonstrated superior performance in various time series tasks compared to traditional recurrent models [15, 16, 17]. Despite these advances, xLSTM remains fundamentally deterministic, limiting its ability to explicitly represent the latent temporal dynamics and stochasticity inherent in many natural processes. This limitation restricts the model's expressiveness when dealing with highly nonlinear and uncertain time series data.

^{*}Corresponding author

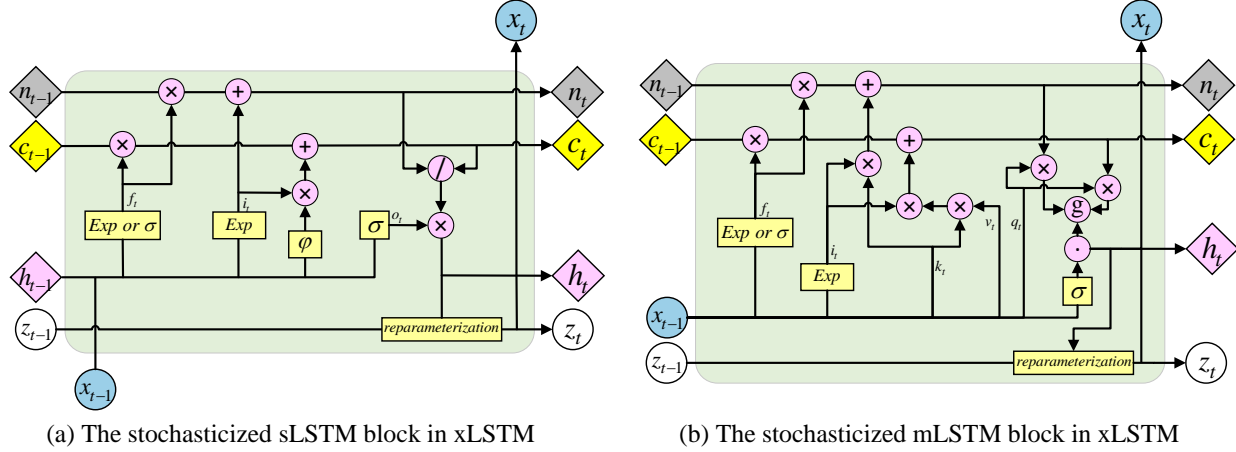


Figure 1: The recurrent unit of StoxLSTM. Diamonds denote deterministic variables, while circles denote stochastic variables. (a) shows the stochasticized sLSTM block, while (b) shows the stochasticized mLSTM block. z_t represents the latent state obtained by stochastic sampling through the reparameterization process.

To overcome these challenges, we propose a **stochastic xLSTM** termed **StoxLSTM** by integrating xLSTM within a specially designed stochastic state space modeling (SSM) framework [18]. Rather than treating RNN and SSM as separate components to be combined [19, 20], our approach integrates latent variable dynamics directly into the recurrent structure, effectively reinterpreting the temporal evolution as a stochastic process parameterized by enhanced xLSTM blocks, as shown in Fig. 1. This formulation allows the model to capture complex hidden temporal patterns and uncertainties that go beyond the capabilities of xLSTM networks and their deterministic variants. By integrating stochastic latent dynamics directly into the recurrent architecture, our approach enhances the representational capacity beyond conventional deterministic frameworks, allowing for more flexible and robust modeling of complex temporal behaviors.

The superiority of the proposed StoxLSTM is verified through extensive experiments across a wide range of publicly available benchmark datasets covering diverse domains such as Electricity, Weather, ETT, Solar, Traffic, PEMS, and ILI [21, 22]. The experimental results demonstrate that StoxLSTM consistently outperforms state-of-the-art baselines across multiple evaluation metrics with better robustness and stronger generalization ability. These results validate the superiority and effectiveness of our stochastic state space reformulation in advancing the modeling power of recurrent architectures for time series forecasting. The main contribution of this work can be concluded as follows:

- To the best of our knowledge, a **stochastic xLSTM**, termed **StoxLSTM**, is proposed for the first time. The StoxLSTM improves the raw deterministic xLSTM architecture by integrating stochastic latent variables into the dynamic recurrent evolutions.
- Efficient parameterization methods of latent temporal dynamics in StoxLSTM is designed. Through the stochasticized xLSTM blocks, the StoxLSTM is enabled to flexibly capture complex, nonlinear, and stochastic dependencies that inherently exists in many time series analysis applications.
- Comprehensive experiments on a variety of public available benchmark datasets are conducted. Experimental results verified that StoxLSTM can achieve consistent and significant performance gain over current state-of-the-art methods. The superiority and effectiveness of the stochastic state space reformulation of xLSTM are validated.

2 Related Work

2.1 Time Series Forecasting Models

Time series forecasting aims to predict future values based on historical observations, and has seen significant advances through various modeling paradigms. Among these, Transformer-based models [23] have attracted extensive attention due to their powerful sequence modeling capabilities. Notable variants include Informer [13], Autoformer [24], Crossformer [25], and FEDformer [26], which improve efficiency and accuracy for long-term TSF. However, recent work such as LTSF-Linear [27] challenges the supremacy of Transformers by demonstrating that simple linear models

can outperform them on long-term TSF. These linear models [27, 28, 29] better preserve temporal order, effectively input longer look-back lengths without overfitting, and benefit from improved embedding strategies, leading to enhanced interpretability [30]. Inspired by these advances, models like iTransformer [31] and PatchTST [32] incorporate linear transformations along the temporal dimension to enhance Transformer-based forecasting.

In parallel, recurrent architectures remain competitive. xLSTM [14] has recently gained prominence due to its ability to capture complex temporal dependencies. Variants such as xLSTMTime [17], P-sLSTM [15], and xLSTM-Mixer [16] have demonstrated superior TSF performance compared to both Transformer- and linear-based models, highlighting the effectiveness of xLSTM in modeling long-range temporal patterns.

2.2 Generative Modeling for Time Series

Generative modeling approaches have emerged as powerful tools for time series analysis, particularly in capturing uncertainty and complex temporal dynamics beyond deterministic predictions. These methods often introduce latent variables or probabilistic frameworks to model the stochastic nature of real-world time series. Classical statistical models such as ARIMA [33], VAR [34] and SSMs [18] have long been used for probabilistic forecasting by modeling trends, seasonality, and inter-variable dependencies. However, these methods often rely on strong assumptions and are limited in their ability to handle nonlinearities and high-dimensional data commonly found in real-world applications.

Recent advances in deep generative modeling have introduced more flexible frameworks that can better capture complex data distributions without restrictive parametric assumptions. Generative adversarial networks (GANs) [35, 36] and diffusion-based models [37, 38] have demonstrated strong capabilities in modeling intricate temporal patterns and generating realistic synthetic sequences. Among these, deep SSMs [19, 11, 39] stand out by explicitly incorporating latent variables to represent hidden states evolving over time, thereby effectively capturing stochastic temporal dependencies. These deep SSMs typically leverage variational inference techniques [40] to approximate intractable posterior distributions, enabling efficient learning and inference. For instance, ProTran [39] combines SSMs with Transformer architectures to model long-term dependencies in a probabilistic manner, achieving strong performance in uncertainty-aware forecasting tasks.

3 Methodology

3.1 Modeling Time series Forecasting with a Deep SSM

Consider a multivariate time series $x_{1:L+T}^C$, where C denotes the number of variables (dimensions), L denotes the look-back length, and T denotes the prediction horizon. Each dimension $x_{1:L+T}^i$ can be treated as an individual univariate time series.

For the univariate time series $x_{1:L+T} = \{x_1, x_2, \dots, x_L, \dots, x_{L+T}\}$, forecasting with deep learning models involves parameterizing the predictive distribution $p_\theta(x_{L+1:L+T}|x_{1:L})$ with network parameters θ . When integrating deep learning with SSMs, latent states $z_{1:L+T}$ are introduced to capture latent dynamics, transforming the predictive distribution into the joint distribution $p_\theta(x_{1:L+T}, z_{1:L+T}|x_{1:L})$.

3.1.1 Dependency Mapping of the Designed SSM

To enable efficient computation and reduce error propagation during forecasting, the generative and inference models in StoxLSTM are designed following a stochastic SSM structure with explicit dependency assumptions, as illustrated in Fig. 2. Specifically, the latent state z_t is modeled as a Markov process, capturing the temporal evolution of latent features—meaning x_t does not depend on previously generated observations but only on the latent state z_t and the known history $x_{1:L}$. Formally, the joint distribution factorizes as:

$$\begin{aligned}
 & p_\theta(x_{1:L+T}, z_{1:L+T}|x_{1:L}) \\
 &= \prod_{t=1}^{L+T} p_\theta(x_t|x_{1:t-1}, z_{1:t}, x_{1:L}) \cdot p_\theta(z_t|x_{1:t-1}, z_{1:t-1}, x_{1:L}) \\
 &= \prod_{t=1}^L p_\theta(x_t|z_t, x_{1:t-1}) \cdot p_\theta(z_t|z_{t-1}, x_{1:t-1}) \cdot \prod_{t=L+1}^{L+T} p_\theta(x_t|z_t, x_{1:L}) \cdot p_\theta(z_t|z_{t-1}, x_{1:L})
 \end{aligned} \tag{1}$$

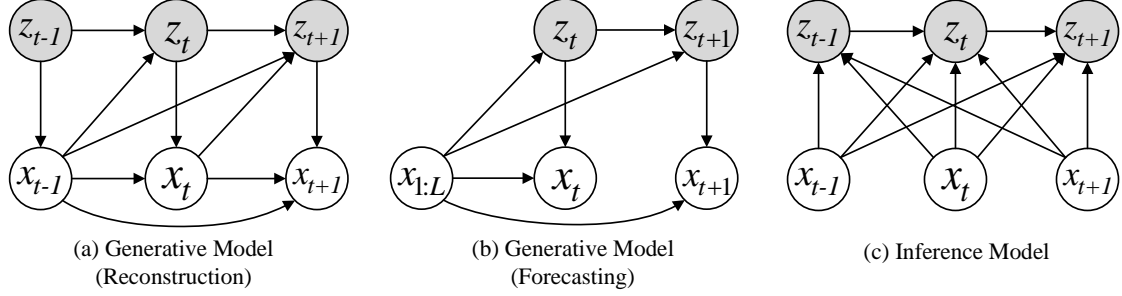


Figure 2: State space models corresponding to the generative model and the inference models in StoxLSTM.

wherein $\prod_{t=1}^L p_\theta(x_t|z_t, x_{1:t-1}) \cdot p_\theta(z_t|z_{t-1}, x_{1:t-1})$ corresponds to the reconstruction of the known history $x_{1:L}$. While $\prod_{t=L+1}^{L+T} p_\theta(x_t|z_t, x_{1:L}) \cdot p_\theta(z_t|z_{t-1}, x_{1:L})$ models the evolution of future states and observations based on the known past $x_{1:L}$.

Correspondingly, the approximate posterior of latent states $z_{1:T}$ with network parameters φ factorizes as:

$$q_\varphi(z_{1:L+T}|x_{1:L+T}) = \prod_{t=1}^{L+T} q_\varphi(z_t|z_{1:t-1}, x_{1:L+T}) = \prod_{t=1}^{L+T} q_\varphi(z_t|z_{t-1}, x_{1:L+T}) \quad (2)$$

3.2 A Stochastic Extend Long Short-term Memory Network

The overall structure of StoxLSTM is illustrated in Fig. 3. StoxLSTM performs channel-independent forecasting for multivariate time series by dividing the multivariate time series into multiple individual univariate sequences. Each univariate sequence $x(i) \in \mathbb{R}^{1 \times L}, i = 1, 2, \dots, C$ is processed independently by the StoxLSTM module, and the outputs are concatenated to form the multivariate prediction $\hat{x} \in \mathbb{R}^{C \times T}$. To address the challenges of modeling long sequences faced by xLSTM [15], each individual sequence is divided into multiple consecutive patches.

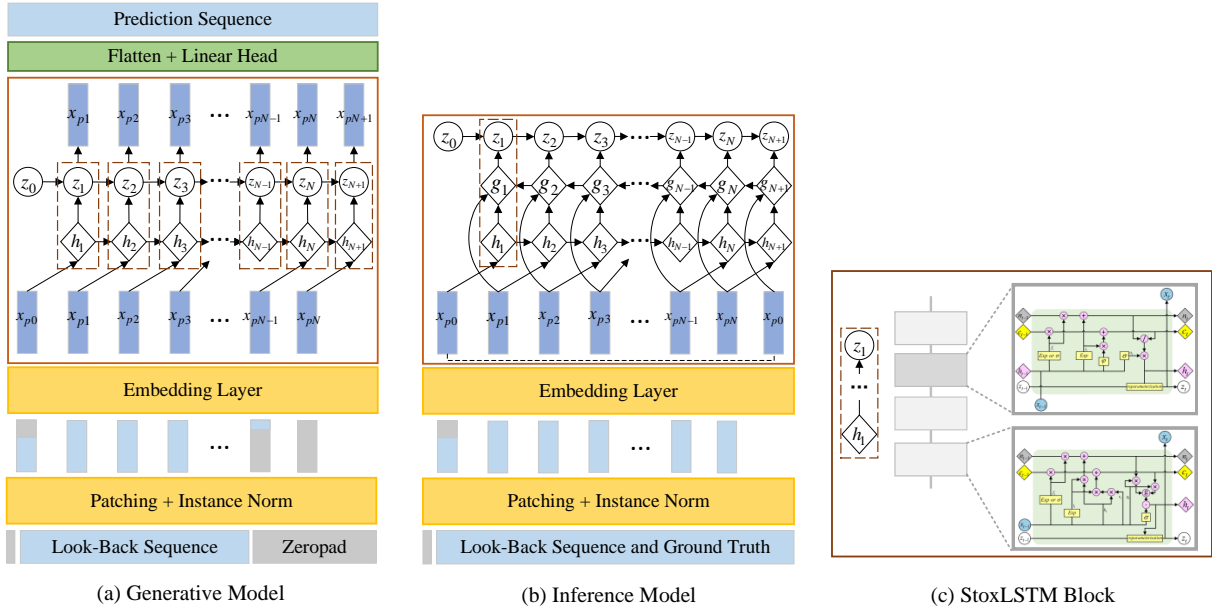


Figure 3: Overall framework of StoxLSTM.

3.2.1 Design of the Recurrent Unit in StoxLSTM

By incorporating stochastic latent variables $z_{1:t}$ into the original xLSTM recurrent unit, as shown in Figs. 1 and 2, StoxLSTM follows the SSM that respects temporal causality, Markovianity, and non-autoregressive dynamics. Specifically, at each time step t , the latent state z_t is modeled as a stochastic variable conditioned on the previous latent state z_{t-1} and the current deterministic hidden state h_t .

Firstly, StosLSTM (the stochasticized sLSTM block in xLSTM, as shown in Fig. 1(a)) forward pass is:

$$\begin{aligned}
 c_t &= f_t' c_{t-1} + i_t' y_t && \text{cell state} \\
 n_t &= f_t' n_{t-1} + i_t' && \text{normalizer state} \\
 h_t &= o_t \tilde{h}_t && \text{hidden state} \\
 z_t &\sim \mathcal{N}(\mu_\theta(h_t, z_{t-1}), \sigma_\theta(h_t, z_{t-1})) && \text{latent state} \\
 x_t &= \varphi(w_z^T z_t + r_z h_t + b_z) && \text{output gate}
 \end{aligned}$$

Here, f_t' and i_t' denote the stabilized forget gate and stabilized input gate, respectively. y_t represents the cell input, and o_t denotes the output gate.

Secondly, StomLSTM (the stochasticized mLSTM block in xLSTM, as shown in Fig. 1(b)) forward pass is:

$$\begin{aligned}
 c_t &= f_t c_{t-1} + i_t v_t k_t^T && \text{cell state} \\
 n_t &= f_t n_{t-1} + i_t k_t && \text{normalizer state} \\
 h_t &= o_t \odot \tilde{h}_t, \quad \tilde{h}_t = C_t q_t / \max\{|n_t^T q_t|, 1\} && \text{hidden state} \\
 z_t &\sim \mathcal{N}(\mu_\theta(h_t, z_{t-1}), \sigma_\theta(h_t, z_{t-1})) && \text{latent state} \\
 x_t &= \varphi(w_z^T z_t + r_z h_t + b_z) && \text{output gate}
 \end{aligned}$$

Here, k_t denotes the key input, q_t denotes the query input, and \odot represents element-wise multiplication.

In both StosLSTM and StomLSTM, we assume that the latent state z_t follows a Gaussian distribution parameterized by a mean $\mu_\theta(h_t, z_{t-1})$ and variance $\sigma_\theta(h_t, z_{t-1})$, both predicted by neural networks. This probabilistic formulation allows the model to capture the inherent uncertainty and stochasticity present in real-world time series data. By sampling z_t from this distribution through the reparameterization block, StoxLSTM is able to represent diverse possible future trajectories, effectively capturing the variability and noise inherent in temporal dynamics. The update of the latent state z_t thus follows the conditional distribution $p(z_t | z_{t-1}, x_{1:t-1})$. Similarly, the output x_t is generated by applying a linear transformation to z_t and h_t , followed by an activation function φ . The generation of x_t follows the conditional distribution $p(x_t | z_t, x_{1:t-1})$.

3.2.2 Generative Model

The generative model evolves according to the factorization in Eq. (1). During preprocessing, zero-padding is applied at both ends of the look-back sequence: padding at the front generates the initial input x_0 with a length equal to the patch stride S , and padding at the end aligns the predicted sequence length T . The padded sequence is then segmented into patches $p_{0:N}$, where $N = \lceil \frac{L+T+S-P}{S} \rceil$, with patch size P . These patches are embedded as:

$$x_{p0:pN} = \text{Embedding}(\text{patching}(\underbrace{[0, \dots, 0]}_S, \underbrace{x_{1:L}, 0, \dots, 0]}_T)) \quad (3)$$

The embedded patches $x_{p0:pN}$ fed into the StoxLSTM recurrent unit to generate latent states $z_{1:N+1}$ and time series patches $x_{p1:pN+1}$:

$$z_{1:N+1}, x_{p1:pN+1} = \text{RecurrentUnit}(x_{p0:pN}) \quad (4)$$

Therefore, during the reconstruction phase, the latent states z_t and observations x_t are generated from the probability distributions $p_\theta(z_t | z_{t-1}, x_{1:t-1})$ and $p_\theta(x_t | z_t, x_{1:t-1})$, respectively. While during the forecasting phase, z_t and x_t are generated from the distributions $p_\theta(z_t | z_{t-1}, x_{1:L})$ and $p_\theta(x_t | z_t, x_{1:L})$, respectively.

The time series patches $x_{p1:pN+1}$ are then flattened and passed through a linear layer to generate the final prediction $x_{L+1:L+T}$:

$$x_{L+1:L+T} = \text{FCL}(\text{Flatten}(x_{p1:pN+1})) \quad (5)$$

where $\text{FCL}(\cdot)$ denotes a fully connected layer.

3.2.3 Inference Model

The inference model follows the factorization in Eq. (2) via a bidirectional recurrent unit [40, 19]. Zero-padding is applied at the front of the sequence $x_{1:L+T}$ with a length equal to the patch stride, followed by patching and embedding:

$$x_{p0:pN} = \text{Embedding}(\text{patching}(\underbrace{[0, \dots, 0]}_S, x_{1:L+T})) \quad (6)$$

The bidirectional recurrent unit processes these embedded patches, producing forward and backward hidden states $h_{1:N+1}$ and $g_{N+1:1}$, which are then used to generate the latent states $z_{1:N+1}$:

$$z_{1:N+1, -} = \text{RecurrentUnit}_{\text{bidirection}}(x_{p0:pN}) \quad (7)$$

The bidirectional recurrent unit enables the latent states z_t to be generated from the approximate posterior distribution $q_\varphi(z_t|z_{t-1}, x_{1:L+T})$. The role of the inference model is to obtain this approximate posterior during training, while during testing, only the generative model is utilized.

3.2.4 Evidence Lower Bound of StoxLSTM

Following the variational inference framework [19, 39, 41, 20, 42], we derive the Evidence Lower Bound (ELBO) as the training objective for StoxLSTM based on the factorization assumptions in Eqs. (1) and (2):

$$\begin{aligned} \log p(x_{1:L+T}|x_{1:L}) &\geq L(\theta, \phi; x_{1:L+T}) = \\ &\sum_{t=1}^L (E_{q_\varphi(z_t|z_{t-1}, x_{1:L+T})} [\log p_\theta(x_t|z_t, x_{1:t-1})] - KL(q_\varphi(z_t|z_{t-1}, x_{1:L+T}) || p_\theta(z_t|z_{t-1}, x_{1:t-1}))) \\ &+ \sum_{t=L+1}^{L+T} (E_{q_\varphi(z_t|z_{t-1}, x_{1:L+T})} [\log p_\theta(x_t|z_t, x_{1:L})] - KL(q_\varphi(z_t|z_{t-1}, x_{1:L+T}) || p_\theta(z_t|z_{t-1}, x_{1:L}))) \end{aligned}$$

Here, $KL(\cdot)$ denotes the KL divergence. This objective encourages the model to reconstruct the observed sequence accurately while maintaining consistency between the inferred latent states and their temporal dynamics. Detailed derivations and implementation details are provided in Appendix A.

3.2.5 Complexity Analysis of StoxLSTM

For a time series $x_{1:L+T}^C$, the time complexity of xLSTM is $O(L + T)$, and its space complexity is $O(1)$ [14]. Considering that StoxLSTM adopts patching and channel independence, its time complexity is $O(C(L + T))$ and the space complexity is $O(1)$. Compared to Transformer-based models, StoxLSTM exhibits lower time and space complexity. However, it still has a relatively large number of parameters. During training, both the inference and generative models are required, but during inference, only the generative model is used, reducing computational time and memory overhead.

4 Experiments

4.1 Time Series Forecasting

4.1.1 Datasets

We employ 9 publicly available datasets to evaluate the performance of our proposed StoxLSTM for long-term time series forecasting. These datasets include: Electricity², Weather³, Solar⁴, Traffic⁵, ILI⁶, and four ETT⁷ datasets (ETTm1, ETTm2, ETTh1, ETTh2). Additionally, we utilize 4 public datasets to assess the performance of short-term time series forecasting, which include: PEMS⁸ (PEMS03, PEMS04, PEMS07, and PEMS08). These datasets have been widely used for benchmarking and are publicly available in [24], [27], [16] and [43]. Detailed dataset information is summarized in Table 1.

²<https://archive.ics.uci.edu/ml/datasets/ElectricityLoadDiagrams20112014>

³<https://www.bgc-jena.mpg.de/wetter/>

⁴<https://github.com/laiguokun/multivariate-time-series-data>

⁵<http://pems.dot.ca.gov>

⁶<https://gis.cdc.gov/grasp/fluvview/fluportaldashboard.html>

⁷<https://github.com/zhouhaoyi/ETDataset>

⁸<http://pems.dot.ca.gov>

Table 1: Dataset detailed descriptions. The dataset size is organized in (Train, Validation, Test).

Datasets	Dim	Horizon	Dataset size	Frequency	Information	Tasks
Weather	21	{96, 192, 336, 720}	(36887, 5270, 10539)	10 min	Weather	Long-term forecasting
Electricity	321	{96, 192, 336, 720}	(18412, 2632, 5260)	Hourly	Electricity	Long-term forecasting
Solar-Energy	137	{96, 192, 336, 720}	(36792, 5256, 10512)	10 min	Electricity	Long-term forecasting
ETTh1, ETTh2	7	{96, 192, 336, 720}	(8640, 2880, 2880)	Hourly	Temperature	Long-term forecasting
ETTm1, ETTm2	7	{96, 192, 336, 720}	(34560, 11520, 11520)	15 min	Temperature	Long-term forecasting
Traffic	862	{96, 192, 336, 720}	(12280, 1756, 3508)	10 min	Transportation	Long-term forecasting
ILI	170	{24, 36, 48, 60}	(676, 97, 193)	7 days	Illness	Long-term forecasting
PEMS03	358	12	(15724, 5241, 5243)	5 min	Transportation	Short-term forecasting
PEMS04	307	12	(10195, 3398, 3399)	5 min	Transportation	Short-term forecasting
PEMS07	883	12	(16934, 5644, 5646)	5 min	Transportation	Short-term forecasting
PEMS08	170	12	(10713, 3571, 3572)	5 min	Transportation	Short-term forecasting

4.1.2 StoxLSTM Configuration

StoxLSTM is configured with a consistent set of hyperparameters across all experiments: Patch size $P = 56$, Stride $S = 24$, model dimension $d_{model} = 64$, and latent dimension $d_{latent} = 16$. Other hyperparameters, including fully connected layer sizes, batch size, learning rate, and dropout rate, are adjusted based on dataset dimensionality and size.

In all experiments, we use mean squared error (MSE) as the reconstruction loss. The loss function of StoxLSTM can be expressed as:

$$Loss_function = \text{MSE}(x_{1:L+T}, \hat{x}_{1:L+T}) + \frac{\beta}{d} \sum_{i=1}^d \left(\log \frac{\sigma_{p_i}}{\sigma_{q_i}} - \frac{1}{2} + \frac{\sigma_{p_i}^2 + (\mu_{q_i} - \mu_{p_i})^2}{2\sigma_{q_i}^2} \right)$$

where $x_{1:L+T}$ denotes the ground truth sequence, and $\hat{x}_{1:L+T}$ represents the prediction from StoxLSTM. The second term corresponds to the KL divergence between two Gaussian distributions. Here, p denotes either $p_\theta(z_t|z_{t-1}, x_{1:L})$ or $p_\theta(z_t|z_{t-1}, x_{1:t-1})$, while q denotes $q_\varphi(z_t|z_{t-1}, x_{1:L+T})$. μ and σ represent the mean and standard deviation of the respective distributions. d is the latent dimension d_{latent} , and i indexes the i -th dimension of the latent variable. The hyperparameter β controls the relative weighting between the reconstruction and KL divergence terms, and is typically set to $\beta = 500$ in our experiments. The RAdam optimizer [44] is employed alongside a cosine annealing learning rate scheduler.

4.1.3 Baselines and Experiment Settings.

We select three types of state-of-the-art models as baselines for long-term and short-term time series forecasting:

Transformer-based: Informer [13], Autoformer [24], Crossformer [25], FEDformer [26], PatchTST [32] and iTransformer [31].

Linear-based: Dlinear [27] and TimeMixer++ [28, 29].

xLSTM-based: xLSTMTime [17], P-sLSTM [15] and xLSTM-Mixer [16].

All models are evaluated under consistent experimental conditions.

For long-term forecasting, the prediction horizons for the ILI dataset are set to $T \in \{24, 36, 48, 60\}$, with StoxLSTM's look-back window fixed at $L = 96$. For all other datasets, the prediction horizons are $T \in \{96, 192, 336, 720\}$, and the look-back window of StoxLSTM is set to $L = 336$. For short-term forecasting, all models are set to $T = 12$ and $L = 96$. Baseline results and look-back length L settings of long-term forecasting are primarily sourced from PatchTST [32], xLSTM-Mixer [16] and TimeMixer++ [29], supplemented by our own experiments where results are unavailable. Evaluation metrics for long-term forecasting include Mean Squared Error (MSE) and Mean Absolute Error (MAE), while short-term forecasting is assessed using MAE, Mean Absolute Percentage Error (MAPE), and Root Mean Squared Error (RMSE). Experiments are conducted on an NVIDIA RTX 3090 GPU (24GB) and 3 NVIDIA A800 GPUs (80GB).

4.1.4 Metrics

To ensure maximum comparability with prior work [32, 16, 29], we adopt the commonly used evaluation metrics for all models. Specifically, long-term forecasting is assessed using mean absolute error (MAE) and MSE. Short-term forecasting is evaluated with MAE, root mean squared error (RMSE), and mean absolute percentage error (MAPE). These metrics are averaged across all variables and calculated as follows:

$$\text{MAE}(\mathbf{y}, \hat{\mathbf{y}}) = \frac{1}{T} \sum_{i=1}^T |y_i - \hat{y}_i| \quad \text{MAPE}(\mathbf{y}, \hat{\mathbf{y}}) = \frac{100}{T} \sum_{i=1}^T \frac{|y_i - \hat{y}_i|}{|y_i| + \varepsilon}$$

$$\text{MSE}(\mathbf{y}, \hat{\mathbf{y}}) = \frac{1}{T} \sum_{i=1}^T (y_i - \hat{y}_i)^2 \quad \text{RMSE}(\mathbf{y}, \hat{\mathbf{y}}) = \sqrt{\frac{1}{T} \sum_{i=1}^T (y_i - \hat{y}_i)^2}$$

wherein \mathbf{y} denotes the ground truth, $\hat{\mathbf{y}}$ denotes the predictions, and ε is a small constant for numerical stability. Additionally, the Continuous Ranked Probability Score (CRPS) evaluation metric is detailed in Appendix B.1.

4.1.5 Results

Table 2 and Table 3 present the results of long- and short-term time series forecasting, respectively. In general, StoxLSTM consistently outperforms all baseline models in nearly all datasets and prediction horizons, achieving the lowest MSE, MAE, MAPE, and RMSE.

Table 2: Long-term time series forecasting results. The best results are in **bold** and the second best are in underline.

Models	StoxLSTM		xLSTM-Mixer		xLSTMTime		P-sLSTM		iTransformer		PatchTST		FEDformer		Informer		Autoformer		Dlinear		TimeMixer++		
Metric	MSE	MAE	MSE	MAE	MSE	MAE	MSE	MAE	MSE	MAE	MSE	MAE	MSE	MAE	MSE	MAE	MSE	MAE	MSE	MAE	MSE	MAE	
Weather	96	0.113 0.168	0.143	0.184	0.144	0.187	0.149	0.208	0.174	0.214	0.149	0.198	0.217	0.296	0.300	0.384	0.266	0.336	0.176	0.237	0.155	0.205	
	192	0.141 0.207	0.186	<u>0.226</u>	0.192	0.236	0.197	0.256	0.221	0.254	0.194	0.241	0.276	0.336	0.598	0.544	0.307	0.367	0.220	0.282	0.201	0.245	
	336	0.162 0.225	0.236	0.266	0.237	0.272	0.249	0.297	0.278	0.296	0.245	0.282	0.339	0.380	0.578	0.523	0.359	0.395	0.265	0.319	0.237	0.265	
	720	0.196 0.255	0.310	0.323	0.313	0.326	0.320	0.350	0.358	0.347	0.314	0.334	0.403	0.428	1.059	0.741	0.419	0.428	0.323	0.362	0.312	0.334	
Electricity	96	0.117 0.223	0.126	0.218	0.128	<u>0.221</u>	0.130	0.226	0.148	0.240	0.129	0.222	0.193	0.308	0.274	0.368	0.201	0.317	0.140	0.237	0.135	0.222	
	192	0.136 0.242	<u>0.144</u>	0.235	0.150	0.243	0.148	0.243	0.162	0.253	0.147	<u>0.240</u>	0.201	0.315	0.296	0.386	0.222	0.334	0.153	0.249	0.147	0.235	
	336	0.144 0.253	<u>0.157</u>	<u>0.250</u>	0.166	0.259	0.165	0.262	0.178	0.269	0.163	0.259	0.214	0.329	0.300	0.394	0.231	0.338	0.169	0.267	0.164	0.245	
	720	0.159 0.270	0.183	0.276	0.185	<u>0.276</u>	0.199	0.293	0.225	0.317	0.197	0.290	0.246	0.355	0.373	0.439	0.254	0.331	0.203	0.301	0.212	0.310	
Solar	96	0.098 0.179	0.227	0.313	0.241	0.306	0.167	0.232	0.203	0.237	0.167	<u>0.224</u>	0.287	0.383	0.200	0.247	0.456	0.446	0.289	0.377	0.171	0.231	
	192	0.124 0.212	0.245	0.328	0.265	0.331	<u>0.180</u>	<u>0.241</u>	0.233	0.261	0.189	0.251	0.278	0.364	0.220	0.251	0.588	0.561	0.319	0.397	0.218	0.263	
	336	0.139 0.224	0.255	0.330	0.267	0.336	<u>0.190</u>	<u>0.248</u>	0.248	0.273	0.193	0.252	0.319	0.397	0.260	0.287	0.595	0.588	0.352	0.415	0.212	0.269	
	720	0.169 0.241	0.257	0.324	0.261	0.324	0.196	<u>0.249</u>	0.249	0.275	0.204	0.269	0.319	0.402	0.244	0.301	0.733	0.633	0.356	0.412	0.212	0.270	
ETTh1	96	0.342 0.398	<u>0.359</u>	0.386	0.368	0.395	0.381	0.405	0.386	0.405	0.370	0.400	0.376	0.419	0.865	0.713	0.449	0.459	0.375	<u>0.399</u>	0.361	0.403	
	192	0.370 0.411	0.402	0.417	<u>0.401</u>	<u>0.416</u>	0.420	0.431	0.441	0.436	0.413	0.429	0.420	0.448	1.008	0.792	0.500	0.482	0.405	0.416	0.416	0.441	
	336	0.379 0.419	0.408	0.429	0.422	0.437	0.456	0.458	0.487	0.458	0.422	0.440	0.459	0.465	1.107	0.809	0.521	0.496	0.439	0.443	0.430	0.434	
	720	0.381 0.422	0.419	0.448	0.441	0.465	0.516	0.512	0.503	0.491	0.447	0.468	0.506	0.507	1.181	0.865	0.514	0.512	0.472	0.490	0.467	0.451	
ETTh2	96	0.238 0.307	0.267	<u>0.329</u>	0.273	0.333	0.320	0.378	0.297	0.349	0.274	0.337	0.346	0.388	3.755	1.525	0.358	0.397	0.289	0.353	0.276	0.328	
	192	0.268 0.340	<u>0.338</u>	<u>0.375</u>	0.340	0.378	0.422	0.442	0.380	0.400	0.341	0.382	0.429	0.441	5.602	1.931	0.456	0.452	0.383	0.418	0.342	0.379	
	336	0.284 0.356	0.367	0.401	0.373	0.403	0.523	0.494	0.428	0.432	0.329	<u>0.384</u>	0.496	0.487	4.721	1.835	0.482	0.486	0.448	0.465	0.346	0.398	
	720	0.316 0.384	0.388	0.424	0.398	0.430	0.946	0.669	0.427	0.445	0.379	0.422	0.463	0.474	3.647	1.625	0.515	0.511	0.605	0.551	0.392	0.415	
ETTh1	96	0.223 0.310	0.275	<u>0.328</u>	0.286	0.335	0.292	0.343	0.334	0.368	0.293	0.346	0.379	0.419	0.672	0.571	0.505	0.475	0.299	0.343	0.310	0.340	
	192	0.261 0.339	0.319	<u>0.354</u>	0.329	0.361	0.329	0.369	0.377	0.391	0.333	0.370	0.426	0.441	0.795	0.669	0.553	0.496	0.335	0.365	0.348	0.362	
	336	0.288 0.357	0.353	0.374	0.358	0.379	0.362	0.391	0.426	0.420	0.369	0.392	0.445	0.459	1.212	0.871	0.621	0.537	0.369	0.386	0.376	0.391	
	720	0.327 0.384	0.409	<u>0.407</u>	0.416	0.411	0.421	0.424	0.491	0.459	0.416	0.420	0.543	0.490	1.166	0.823	0.671	0.561	0.425	0.421	0.440	0.423	
ETTh2	96	0.125 0.224	0.157	<u>0.244</u>	0.164	0.250	0.238	0.302	0.180	0.264	0.166	0.256	0.203	0.287	0.365	0.453	0.255	0.339	0.167	0.260	0.170	0.245	
	192	0.164 0.259	0.213	<u>0.285</u>	0.218	0.288	0.337	0.376	0.250	0.309	0.223	0.296	0.269	0.328	0.533	0.563	0.281	0.340	0.224	0.303	0.229	0.291	
	336	0.192 0.285	0.269	<u>0.322</u>	0.271	0.322	0.444	0.438	0.311	0.348	0.274	0.329	0.325	0.366	1.363	0.887	0.339	0.372	0.281	0.342	0.303	0.343	
	720	0.277 0.349	0.351	0.377	0.361	0.380	0.488	0.482	0.412	0.407	0.362	0.385	0.421	0.415	3.379	1.388	0.422	0.419	0.397	0.421	0.373	0.399	
Traffic	96	0.333 0.258	<u>0.351</u>	0.236	0.358	0.242	0.576	0.332	0.395	0.268	0.360	0.249	0.587	0.366	0.719	0.391	0.613	0.388	0.410	0.282	0.392	0.253	
	192	0.426	0.311	0.377	0.241	0.378	<u>0.253</u>	0.595	0.342	0.417	0.276	0.379	0.256	0.604	0.373	0.696	0.379	0.616	0.382	0.423	0.287	0.402	0.258
	336	0.449	0.320	0.394	0.250	0.392	<u>0.261</u>	0.604	0.345	0.433	0.283	0.392	0.264	0.621	0.383	0.777	0.420	0.622	0.337	0.436	0.296	0.428	0.263
	720	0.469	0.336	0.439	0.283	0.434	0.287	0.630	0.357	0.467	0.302	0.432	0.286	0.626	0.382	0.864	0.472	0.660	0.408	0.466	0.315	0.441	0.282
ILI	24	0.930 0.583	1.351	0.707	1.514	0.694	3.964	1.309	1.834	0.883	1.319	0.754	3.228	1.260	4.657	1.449	2.906	1.182	2.215	1.081	1.811	0.823	
	36	1.181 0.669	<u>1.408</u>	<u>0.712</u>	1.519	0.722	4.095	1.330	1.742	0.870	1.579	0.870	2.679	1.080	4.650	1.463	2.585	1.038	1.963	0.963	1.763	0.835	
	48	1.283 0.738	<u>1.434</u>	<u>0.721</u>	1.500	0.725	4.097	1.326	1.996	0.815	1.553	0.815	2.622	1.078	5.004	1.542	3.024	1.145	2.130	1.024	1.705	0.818	
	60	1.385 0.769	1.512	0.737	1.418	0.715	4.355	1.384	1.806	0.788	1.470	0.788	2.857	1.157	5.071	1.543	2.761	1.114	2.368	1.096	1.708	0.839	
Wins	33	27	1	6	1	1	0	0	0	0	2	0	0	0	0	0	0	0	0	0	0	3	

Table 3: Short-term time series forecasting results. The best results are in **bold** and the second best are in underline. The prediction length is set to 12.

Models	StoxLSTM	xLSTM-Mixer	P-sLSTM	iTransformer	PatchTST	Crossformer	Autoformer	FEDformer	Dlinear	TimeMixer	TimeMixer++
PEMS03	MAE	9.74	15.71	17.15	16.72	18.95	15.64	18.08	19.00	19.70	14.63
	MAPE	9.59	14.92	16.56	15.81	17.29	15.74	18.75	18.35	11.54	<u>13.43</u>
	RMSE	14.65	24.82	27.68	27.81	30.15	25.56	27.82	30.05	32.35	23.28
PEMS04	MAE	14.59	24.61	23.01	21.81	24.86	20.38	25.00	26.51	24.62	19.21
	MAPE	9.25	15.48	14.44	13.42	16.65	12.84	16.70	16.76	16.12	12.53
	RMSE	23.48	38.92	35.92	33.91	40.46	32.41	38.02	41.82	39.51	30.92
PEMS07	MAE	14.36	27.98	23.54	23.01	27.87	22.79	26.92	27.92	28.65	20.57
	MAPE	6.32	12.20	9.78	10.02	12.69	9.41	11.83	12.29	12.15	<u>8.62</u>
	RMSE	22.34	43.92	37.70	35.56	42.56	35.61	40.60	42.29	45.02	33.59
PEMS08	MAE	12.55	16.56	17.20	17.94	20.35	17.38	20.47	20.56	20.26	15.22
	MAPE	7.79	10.24	10.87	10.93	13.15	10.80	12.27	12.41	12.09	<u>9.67</u>
	RMSE	19.45	26.56	27.32	27.88	31.04	27.34	31.52	32.97	32.38	24.26

In long-term forecasting tasks, xLSTM-based models generally demonstrate superior performance compared to Transformer-based and Linear-based models, highlighting the strength of recurrent architectures like xLSTM in capturing long-range temporal dependencies. Among these, StoxLSTM achieves the best results. For instance, on the Weather dataset, StoxLSTM attains an average MSE of 0.161 across different prediction horizons, which is **26.5%** lower than the xLSTM-Mixer's average MSE of 0.219. Similarly, on the Electricity dataset, StoxLSTM achieves an average MSE of 0.139, outperforming xLSTM-Mixer's 0.153 by **9.1%**, further demonstrating its consistent advantage. Notably, StoxLSTM maintains this leading performance across other datasets such as Solar, ETTh1, and ETM1, reflecting its robustness and generalizability in diverse long-term forecasting scenarios.

In short-term forecasting, although Linear-based models show competitive results, StoxLSTM still surpasses them by a significant margin. Specifically, across four traffic datasets (PEMS03, PEMS04, PEMS07, and PEMS08), StoxLSTM achieves an average MAE of 12.81, outperforming the best Linear-based model, TimeMixer++, which records an MAE of 15.91, representing a **19.49%** improvement. Furthermore, StoxLSTM attains an average MAPE of 8.24, which is **18.25%** lower than TimeMixer++'s 10.08. In terms of RMSE, StoxLSTM achieves 19.98 on average, outperforming TimeMixer++'s 27.03 by **26.08%**. These consistent improvements across multiple metrics and datasets underscore StoxLSTM's effectiveness in capturing short-term temporal patterns with high accuracy. Some of the forecasting results are shown in Figs. 4 to 6.

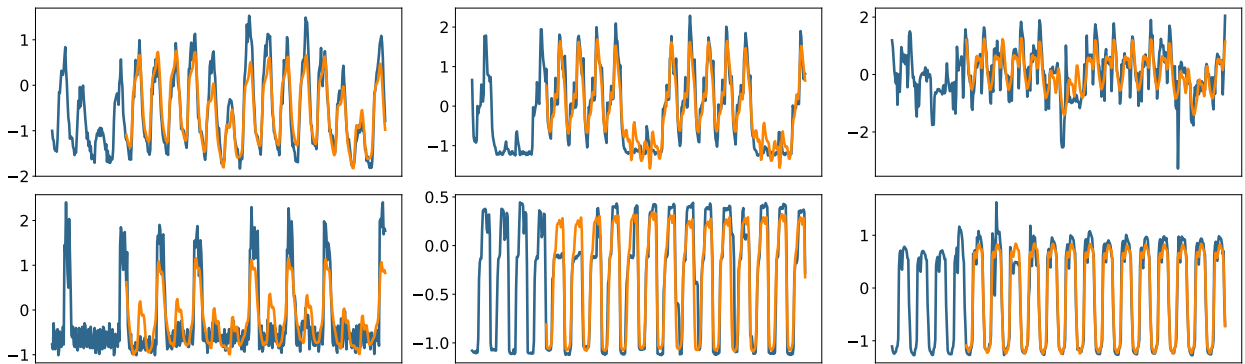


Figure 4: The real and forecasting sequences of the last 6 out of 321 time series from the electricity dataset are shown. The orange line denotes the forecasted values generated by StoxLSTM, while the blue line represents the ground truth. The prediction horizon is set to 336 time steps.

Overall, these results demonstrate that StoxLSTM consistently delivers state-of-the-art accuracy across both short- and long-term forecasting tasks, validating its effectiveness and robustness in diverse time series forecasting scenarios. Supplementary experimental details are provided in B.2.

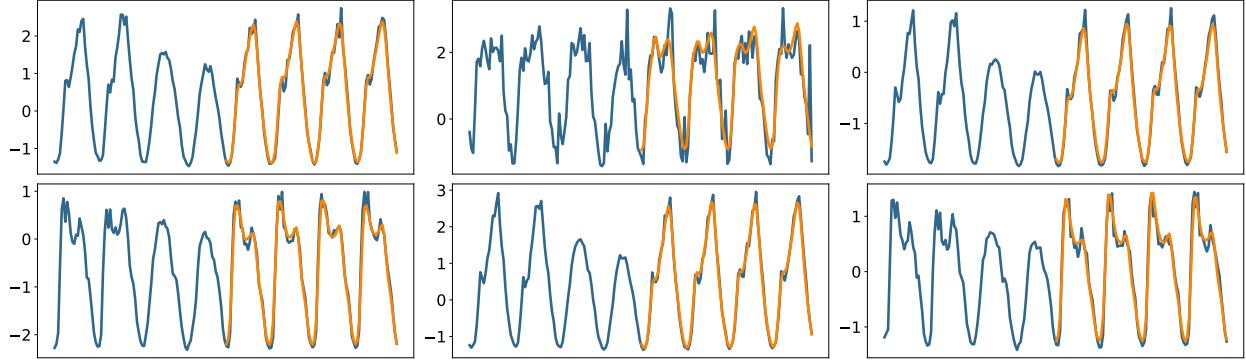


Figure 5: The real and forecasting sequences of the last 6 out of 862 time series from the Traffic dataset are shown. The orange line denotes the forecasted values generated by StoxLSTM, while the blue line represents the ground truth. The prediction horizon is set to 96 time steps.

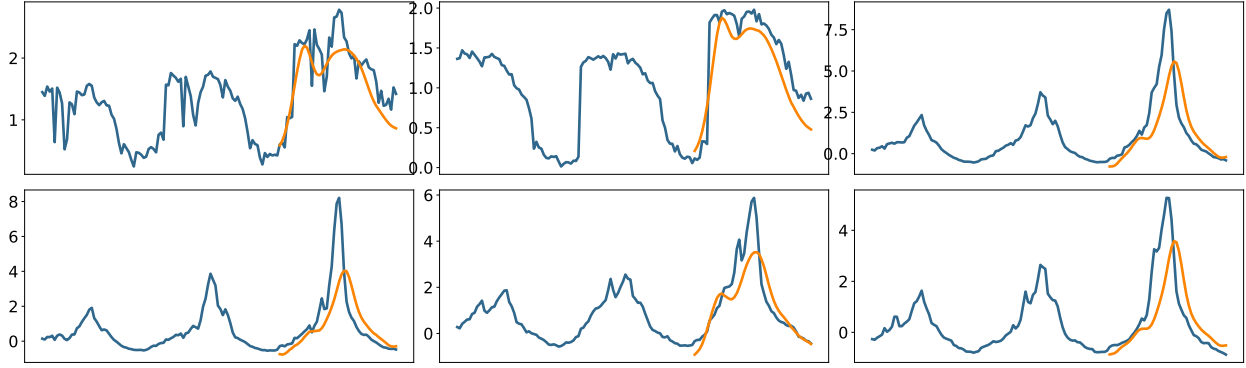


Figure 6: The real and forecasting sequences of the last 6 out of 170 time series from the electricity dataset are shown. The orange line denotes the forecasted values generated by StoxLSTM, while the blue line represents the ground truth. The prediction horizon is set to 48 time steps.

4.2 Model Analysis

4.2.1 Ablation Study.

We study the effect of patching combined with channel independence (P + CI), series decomposition (SD), stochastic latent variables (stochastic), and the SSM structure on forecasting performance, with results summarized in Table 4. P-sLSTM is employed as a baseline to compare against the SSM design integrated within StoxLSTM. For the model without patching and channel independence, the look-back length is reduced to 96 steps (compared to 336 steps for the other models) to prevent overfitting and reduce training time and memory consumption. Additionally, xLSTM-Mixer is included as the state-of-the-art benchmark for xLSTM-based models.

Experimental results clearly demonstrate that all components—series decomposition, patching, channel independence, stochastic latent variables, and the SSM structure—contribute positively to the overall performance of StoxLSTM. Focusing first on the SSM modeling aspect, both the original StoxLSTM and its variants without stochastic latent variables (w/o Stochastic) and without series decomposition (w/o SD) consistently outperform P-sLSTM across all experiments, achieving lower MSE and MAE. This confirms that the state space model enhancement to the xLSTM architecture plays a crucial role in improving forecasting performance. Moreover, compared to the w/o Stochastic variant, StoxLSTM with stochastic latent variables generally achieves better and more stable prediction results, indicating that modeling latent states as random variables better captures the underlying temporal dependencies in time series data and enhances robustness. In contrast, the model variant without patching and channel independence exhibits notable instability: while it achieves excellent results in certain scenarios, its performance deteriorates significantly in others. This suggests that patching and channel independence not only improve robustness but also enable the model to effectively handle longer look-back lengths under constrained computational and memory resources, thereby reducing the risk of overfitting.

Table 4: Ablation studies on StoxLSTM are conducted with 5 variants: (a) original StoxLSTM; (b) StoxLSTM without stochastic latent variables, where the latent state z_t is generated deterministically without random Gaussian sampling (w/o stochastic); (c) StoxLSTM without patching and channel independence methods (w/o P + CI); (d) StoxLSTM without the series decomposition block (w/o SD); and (e) P-sLSTM, which incorporates P + CI and SD but does not apply the SSM enhancement to the xLSTM architecture.

Models	StoxLSTM		w/o stochastic		w/o P + CI		w/o SD		P-sLSTM		xLSTM-Mixer		
Metric	MSE	MAE	MSE	MAE	MSE	MAE	MSE	MAE	MSE	MAE	MSE	MAE	
Weather	96	0.113	0.168	0.113	0.169	0.106	0.163	0.121	0.180	0.149	0.208	0.143	0.184
	192	0.141	0.207	<u>0.139</u>	<u>0.202</u>	0.128	0.188	0.144	0.209	0.197	0.256	0.221	0.254
	336	<u>0.162</u>	0.225	0.163	0.226	0.156	0.220	0.166	0.230	0.249	0.297	0.236	0.266
	720	0.196	0.255	0.198	0.260	<u>0.206</u>	<u>0.267</u>	0.212	0.266	0.320	0.350	0.310	0.323
ETM1	96	0.223	0.310	0.229	0.315	0.304	0.375	0.253	0.336	0.292	0.343	0.275	0.184
	192	0.261	0.339	<u>0.265</u>	<u>0.340</u>	0.494	0.461	0.275	0.351	0.329	0.369	0.319	0.354
	336	0.288	0.357	0.291	<u>0.358</u>	0.592	0.499	<u>0.290</u>	0.360	0.362	0.391	0.353	0.370
	720	0.327	0.384	0.329	<u>0.385</u>	0.645	0.526	<u>0.328</u>	0.385	0.421	0.424	0.409	0.407
Electricity	96	0.117	0.223	<u>0.120</u>	<u>0.229</u>	0.357	0.421	0.151	0.260	0.130	0.226	0.126	0.218
	192	0.136	0.242	<u>0.136</u>	<u>0.244</u>	0.454	0.498	0.152	0.261	0.148	0.243	0.144	0.235
	336	0.144	0.253	<u>0.146</u>	<u>0.255</u>	0.621	0.608	0.158	0.268	0.165	0.262	0.157	0.250
	720	0.159	0.270	<u>0.161</u>	<u>0.274</u>	0.699	0.668	0.162	0.278	0.199	0.293	0.183	0.276

4.2.2 Representational Capacity of the Latent States.

Fig. 7 presents heatmaps of 4 tensor groups— $x_{1:N}$, $x_{p1:pN}$, $z_{1:N}$, and $h_{1:N}$ —extracted from a trained StoxLSTM model while forecasting a specific instance from the Electricity dataset. This instance corresponds to the seasonal component obtained after the series decomposition block. Fig. 7(a) illustrates the heatmaps during the processing by the generative model, while Fig. 7(b) displays those from the inference model.

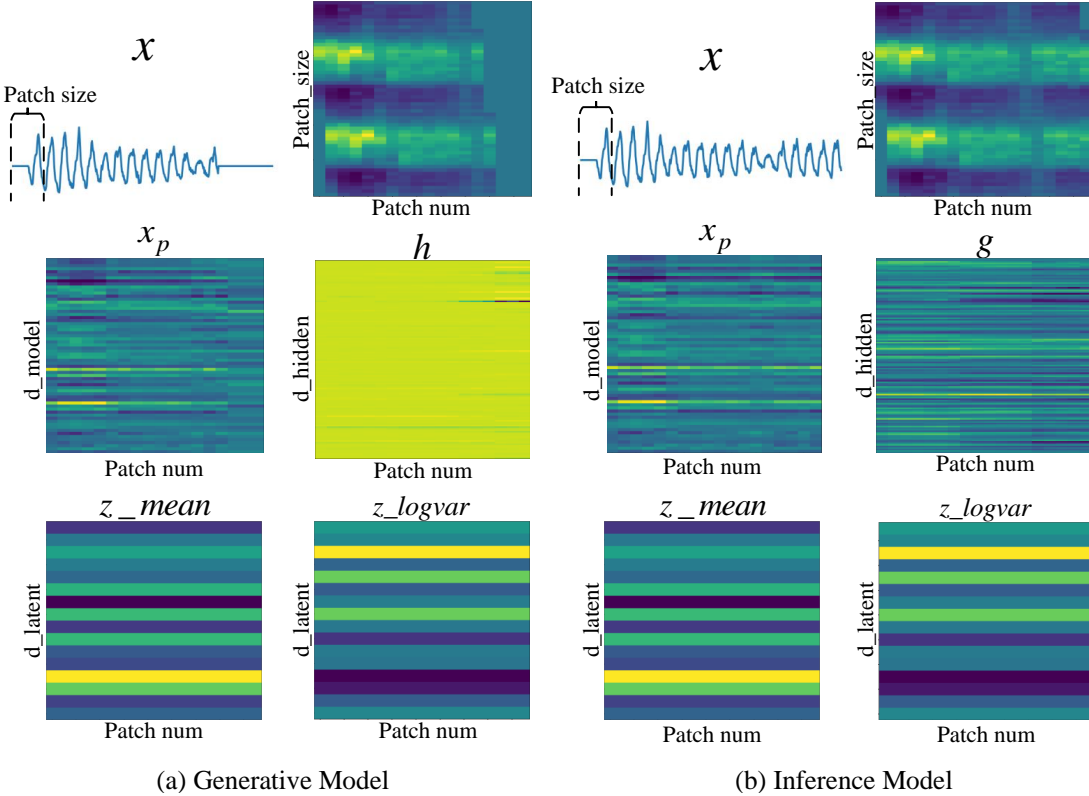


Figure 7: Heatmaps of four tensor groups— x , x_p , z , and h —from StoxLSTM when predicting a specific instance in the Electricity dataset. Different colors indicate different values, with brighter colors corresponding to larger values.

Within the inference model, values of $x_{p1:pN}$ and $g_{1:N}$ exhibit limited variation across patches but display noticeable differences across dimensions within each patch. The latent states effectively capture this pattern: both $z_mean_{1:N}$ and $z_logvar_{1:N}$ remain relatively stable across patches while preserving significant variability across dimensions. This suggests that the latent representation encodes consistent temporal patterns while retaining important feature-level distinctions.

Notably, through variational inference, the latent states learned by the generative model similarly reflect these characteristics—showing near-uniformity across patches alongside meaningful variation across dimensions within each patch. Such a well-structured latent representation, combined with the hidden states $h_{1:N}$, offers a comprehensive and informative summary of the time series, thereby supporting accurate and robust forecasting.

As demonstrated in Fig. 7, the variational inference training converges effectively, and the latent states successfully capture the underlying temporal features of the data. This visualization not only validates the model’s ability to learn meaningful representations but also highlights the interpretability of the latent space in modeling complex temporal dynamics.

5 Conclusion

In this paper, we propose StoxLSTM, a novel stochastic variant of the original xLSTM architecture. By integrating a designed SSM, StoxLSTM effectively captures the dynamic evolution of time series data. Our model demonstrates a strong capability in both long- and short-term forecasting tasks. Extensive experiments on multiple publicly available benchmark datasets show that StoxLSTM consistently outperforms existing state-of-the-art methods in terms of prediction accuracy and robustness. These results validate the effectiveness of combining the xLSTM framework with the SSM design to enhance temporal modeling. Future work will focus on further optimizing the model architecture and improving computational efficiency.

6 Acknowledgement

This work was supported by the National Natural Science Foundation (NSFC) of China under Grant 62301031.

A ELBO Derivation of StoxLSTM

The KL divergence between the approximate posterior probability $q_\varphi(z_{1:L+T}|x_{1:L+T})$ and the posterior probability $p(z_{1:L+T}|x_{1:L+T})$ in StoxLSTM is derived as follows:

$$\begin{aligned}
 & \text{KL}(q_\varphi(z_{1:L+T}|x_{1:L+T}) \| p(z_{1:L+T}|x_{1:L+T})) \\
 &= \mathbb{E}_{q_\varphi(z_{1:L+T}|x_{1:L+T})} [\log q_\varphi(z_{1:L+T}|x_{1:L+T}) - \log p(z_{1:L+T}|x_{1:L+T})] \\
 &= \mathbb{E}_{q_\varphi(z_{1:L+T}|x_{1:L+T})} [\log q_\varphi(z_{1:L+T}|x_{1:L+T}) - \log p(z_{1:L+T}|x_{1:L+T}, x_{1:L})] \\
 &= \mathbb{E}_{q_\varphi(z_{1:L+T}|x_{1:L+T})} [\log q_\varphi(z_{1:L+T}|x_{1:L+T}) - \log p(x_{1:L+T}, z_{1:L+T}|x_{1:L}) + \log p(x_{1:L+T}|x_{1:L})] \\
 &= \mathbb{E}_{q_\varphi(z_{1:L+T}|x_{1:L+T})} [\log q_\varphi(z_{1:L+T}|x_{1:L+T}) - \log p(x_{1:L+T}, z_{1:L+T}|x_{1:L})] + \log p(x_{1:L+T}|x_{1:L})
 \end{aligned}$$

Then, $q_\varphi(z_{1:L+T}|x_{1:L+T})$ and $p(x_{1:L+T}, z_{1:L+T}|x_{1:L})$ can be factorized over time according to Eq. (1) and (2):

$$\begin{aligned}
 & \mathbb{E}_{q_\varphi(z_{1:L+T}|x_{1:L+T})} [\log q_\varphi(z_{1:L+T}|x_{1:L+T}) - \log p(x_{1:L+T}, z_{1:L+T}|x_{1:L})] + \log p(x_{1:L+T}|x_{1:L}) \\
 &= \sum_{t=1}^{L+T} \mathbb{E}_{q_\varphi(z_{1:L+T}|x_{1:L+T})} [\log q_\varphi(z_t|z_{1:t-1}, x_{1:L+T}) - \log p_\theta(z_t|x_{1:t-1}, z_{1:t-1}, x_{1:L}) - \log p_\theta(x_t|x_{1:t-1}, z_{1:t}, x_{1:L})] \\
 &\quad + \log p(x_{1:L+T}|x_{1:L}) \\
 &= \sum_{t=1}^{L+T} \mathbb{E}_{q_\varphi(z_{1:L+T}|x_{1:L+T})} [\log q_\varphi(z_t|z_{1:t-1}, x_{1:L+T}) - \log p_\theta(z_t|x_{1:t-1}, z_{1:t-1}, x_{1:L})] \\
 &\quad - \sum_{t=1}^{L+T} \mathbb{E}_{q_\varphi(z_{1:L+T}|x_{1:L+T})} [\log p_\theta(x_t|x_{1:t-1}, z_{1:t}, x_{1:L})] + \log p(x_{1:L+T}|x_{1:L}) \\
 &= \sum_{t=1}^{L+T} \mathbb{E}_{q_\varphi(z_{t+1:L+T}|x_{1:L+T})} \left[\mathbb{E}_{q_\varphi(z_{1:t-1}|x_{1:L+T})} \left[\mathbb{E}_{q_\varphi(z_t|z_{1:t-1}, x_{1:L+T})} [\log q_\varphi(z_t|z_{1:t-1}, x_{1:L+T}) - \log p_\theta(z_t|x_{1:t-1}, z_{1:t-1}, x_{1:L})] \right] \right] \\
 &\quad - \sum_{t=1}^{L+T} \mathbb{E}_{q_\varphi(z_{t+1:L+T}|x_{1:L+T})} \left[\mathbb{E}_{q_\varphi(z_{1:t-1}|x_{1:L+T})} \left[\mathbb{E}_{q_\varphi(z_t|z_{1:t-1}, x_{1:L+T})} [\log p_\theta(x_t|x_{1:t-1}, z_{1:t}, x_{1:L})] \right] \right] \\
 &\quad + \log p(x_{1:L+T}|x_{1:L})
 \end{aligned}$$

Moreover, based on the following expression for the KL divergence:

$$\begin{aligned}
 & \text{KL}(q_\varphi(z_t|z_{1:t-1}, x_{1:L+T}) \| p_\theta(z_t|x_{1:t-1}, z_{1:t-1}, x_{1:L})) \\
 &= \mathbb{E}_{q_\varphi(z_t|z_{1:t-1}, x_{1:L+T})} [\log q_\varphi(z_t|z_{1:t-1}, x_{1:L+T}) - \log p_\theta(z_t|x_{1:t-1}, z_{1:t-1}, x_{1:L})]
 \end{aligned}$$

The above expression can be simplified as follows:

$$\begin{aligned}
 & \sum_{t=1}^{L+T} \mathbb{E}_{q_\varphi(z_{t+1:L+T}|x_{1:L+T})} \left[\mathbb{E}_{q_\varphi(z_{1:t-1}|x_{1:L+T})} \left[\mathbb{E}_{q_\varphi(z_t|z_{1:t-1}, x_{1:L+T})} \left[\log q_\varphi(z_t|z_{1:t-1}, x_{1:L+T}) - \log p_\theta(z_t|x_{1:t-1}, z_{1:t-1}, x_{1:L}) \right] \right] \right] \\
 & - \sum_{t=1}^{L+T} \mathbb{E}_{q_\varphi(z_{t+1:L+T}|x_{1:L+T})} \left[\mathbb{E}_{q_\varphi(z_{1:t-1}|x_{1:L+T})} \left[\mathbb{E}_{q_\varphi(z_t|z_{1:t-1}, x_{1:L+T})} \left[\log p_\theta(x_t|x_{1:t-1}, z_{1:t}, x_{1:L}) \right] \right] \right] + \log p(x_{1:L+T}|x_{1:L}) \\
 = & \sum_{t=1}^{L+T} \mathbb{E}_{q_\varphi(z_{t+1:L+T}|x_{1:L+T})} \left[\mathbb{E}_{q_\varphi(z_{1:t-1}|x_{1:L+T})} \left[\text{KL}(q_\varphi(z_t|z_{1:t-1}, x_{1:L+T}) \| p_\theta(z_t|x_{1:t-1}, z_{1:t-1}, x_{1:L})) \right] \right] \\
 & - \sum_{t=1}^{L+T} \mathbb{E}_{q_\varphi(z_{t+1:L+T}|x_{1:L+T})} \left[\mathbb{E}_{q_\varphi(z_{1:t-1}|x_{1:L+T})} \left[\mathbb{E}_{q_\varphi(z_t|z_{1:t-1}, x_{1:L+T})} \left[\log p_\theta(x_t|x_{1:t-1}, z_{1:t}, x_{1:L}) \right] \right] \right] + \log p(x_{1:L+T}|x_{1:L}) \\
 = & \sum_{t=1}^{L+T} \mathbb{E}_{q_\varphi(z_{t+1:L+T}|x_{1:L+T})} \left[\mathbb{E}_{q_\varphi(z_{1:t-1}|x_{1:L+T})} \left[\text{KL}(q_\varphi(z_t|z_{1:t-1}, x_{1:L+T}) \| p_\theta(z_t|x_{1:t-1}, z_{1:t-1}, x_{1:L})) \right. \right. \\
 & \left. \left. - \mathbb{E}_{q_\varphi(z_t|z_{1:t-1}, x_{1:L+T})} [\log p_\theta(x_t|x_{1:t-1}, z_{1:t}, x_{1:L})] \right] \right] + \log p(x_{1:L+T}|x_{1:L})
 \end{aligned}$$

Rearranging the above equation:

$$\begin{aligned}
 \log p(x_{1:L+T}|x_{1:L}) &= \text{KL}(q_\varphi(z_{1:L+T}|x_{1:L+T}) \| p(z_{1:L+T}|x_{1:L+T})) \\
 &+ \sum_{t=1}^{L+T} \mathbb{E}_{q_\varphi(z_{t+1:L+T}|x_{1:L+T})} \left[\mathbb{E}_{q_\varphi(z_{1:t-1}|x_{1:L+T})} \left[\mathbb{E}_{q_\varphi(z_t|z_{1:t-1}, x_{1:L+T})} \left[\log p_\theta(x_t|x_{1:t-1}, z_{1:t}, x_{1:L}) \right. \right. \right. \\
 & \left. \left. \left. - \text{KL}(q_\varphi(z_t|z_{1:t-1}, x_{1:L+T}) \| p_\theta(z_t|x_{1:t-1}, z_{1:t-1}, x_{1:L})) \right] \right] \right]
 \end{aligned}$$

Since $\text{KL}(q_\varphi(z_{1:L+T}|x_{1:L+T}) \| p(z_{1:L+T}|x_{1:L+T}))$ is non-negative, we can derive the ELBO as follows:

$$\begin{aligned}
 \log p(x_{1:L+T}|x_{1:L}) &\geq L(\theta, \phi; x_{1:L+T}) = \sum_{t=1}^{L+T} \left(\mathbb{E}_{q_\varphi(z_t|z_{1:t-1}, x_{1:L+T})} [\log p_\theta(x_t|x_{1:t-1}, z_{1:t}, x_{1:L})] \right. \\
 & \left. - \text{KL}(q_\varphi(z_t|z_{1:t-1}, x_{1:L+T}) \| p_\theta(z_t|x_{1:t-1}, z_{1:t-1}, x_{1:L})) \right)
 \end{aligned}$$

Finally, based on the assumptions in Eq. (1) and (2), the ELBO of StoxLSTM can be derived as:

$$\begin{aligned}
 \log p(x_{1:L+T}|x_{1:L}) &\geq L(\theta, \phi; x_{1:L+T}) = \\
 & \sum_{t=1}^L \left(\mathbb{E}_{q_\varphi(z_t|z_{t-1}, x_{1:L+T})} [\log p_\theta(x_t|z_t, x_{1:t-1})] - \text{KL}(q_\varphi(z_t|z_{t-1}, x_{1:L+T}) \| p_\theta(z_t|z_{t-1}, x_{1:t-1})) \right) \\
 & + \sum_{t=L+1}^{L+T} \left(\mathbb{E}_{q_\varphi(z_t|z_{t-1}, x_{1:L+T})} [\log p_\theta(x_t|z_t, x_{1:L})] - \text{KL}(q_\varphi(z_t|z_{t-1}, x_{1:L+T}) \| p_\theta(z_t|z_{t-1}, x_{1:L})) \right)
 \end{aligned}$$

B Supplementary Experiments

B.1 CRPS Evaluation Metric

Generative time series forecasting can also use the Continuous Ranked Probability Score (CRPS) to evaluate the prediction results. CRPS is computed by comparing the ground truth with the cumulative distribution function (CDF):

$$\text{CRPS}(F, y) = \int (F(x) - 1_{\{x \geq y\}})^2 dx, \quad 1_{\{x \geq y\}} = \begin{cases} 0, & \text{if } x < y \\ 1, & \text{if } x \geq y \end{cases}$$

For point forecasting models, the point prediction can be treated as a degenerate CDF. Substituting into the formula and simplifying yields:

$$\text{CRPS}(1_{\{x \geq \hat{y}\}}, y) = \int (1_{\{x \geq \hat{y}\}} - 1_{\{x \geq y\}})^2 dx = \begin{cases} \int_{\hat{y}}^y 1 dx, & y > \hat{y} \\ \int_y^{\hat{y}} 1 dx, & \hat{y} \geq y \end{cases} = |y - \hat{y}|$$

indicating that CRPS for point forecasts is equivalent to MAE.

Table 5: Long-term time series forecasting results. The best results are in **bold** and the second best are in underline. The evaluation metric is CRPS.

Models	StoxLSTM	xLSTM-Mixer	xLSTMTime	P-sLSTM	iTransformer	PatchTST	FEDformer	Informer	Autoformer	Dlinear	TimeMixer++	
Weather	96	0.167	<u>0.184</u>	0.187	0.208	0.214	0.198	0.296	0.384	0.336	0.237	0.205
	192	0.206	<u>0.226</u>	0.236	0.256	0.254	0.241	0.336	0.544	0.367	0.282	0.245
	336	0.225	<u>0.266</u>	0.272	0.297	0.296	0.282	0.380	0.523	0.395	0.319	0.265
	720	0.254	<u>0.323</u>	0.326	0.350	0.347	0.334	0.428	0.741	0.428	0.362	0.334
Electricity	96	0.223	0.218	<u>0.221</u>	0.226	0.240	0.222	0.308	0.368	0.317	0.237	0.222
	192	<u>0.242</u>	0.235	0.243	0.243	0.253	0.240	0.315	0.386	0.334	0.249	0.235
	336	<u>0.253</u>	0.250	0.259	0.262	0.269	0.259	0.329	0.394	0.338	0.267	0.245
	720	0.270	<u>0.276</u>	0.276	0.293	0.317	0.290	0.355	0.439	0.331	0.301	0.310
Solar	96	0.178	0.313	<u>0.306</u>	0.232	0.237	0.224	0.383	0.247	0.446	0.377	0.231
	192	0.212	0.328	0.331	<u>0.241</u>	0.261	<u>0.251</u>	0.364	<u>0.251</u>	0.561	0.397	0.263
	336	0.223	0.330	0.336	<u>0.248</u>	0.273	0.252	0.397	0.287	0.588	0.415	0.269
	720	0.241	0.324	0.324	<u>0.249</u>	0.275	0.269	0.402	0.301	0.633	0.412	0.270
ETTh1	96	<u>0.396</u>	0.386	0.395	0.405	0.405	0.400	0.419	0.713	0.459	0.399	0.403
	192	0.407	0.417	<u>0.416</u>	0.431	0.436	0.429	0.448	0.792	0.482	0.416	0.441
	336	0.412	<u>0.429</u>	0.437	0.458	0.458	0.440	0.465	0.809	0.496	<u>0.443</u>	0.434
	720	0.421	<u>0.448</u>	0.465	0.512	0.491	0.468	0.507	0.865	0.512	0.490	0.451
ETTh2	96	0.305	0.329	0.333	0.378	0.349	0.337	0.388	1.525	0.397	0.353	<u>0.328</u>
	192	0.337	<u>0.375</u>	0.378	0.442	0.400	0.382	0.439	1.931	0.452	0.418	0.379
	336	0.354	0.401	0.403	0.494	0.432	<u>0.384</u>	0.487	1.835	0.486	0.465	0.398
	720	0.382	0.424	0.430	0.669	0.445	0.422	0.474	1.625	0.511	0.551	<u>0.415</u>
ETM1	96	0.307	<u>0.328</u>	0.335	0.343	0.368	0.346	0.419	0.571	0.475	0.343	0.334
	192	0.336	<u>0.354</u>	0.361	0.369	0.391	0.370	0.441	0.669	0.496	0.365	0.362
	336	0.356	<u>0.374</u>	0.379	0.391	0.420	0.392	0.459	0.871	0.537	0.386	0.391
	720	0.384	<u>0.407</u>	0.411	0.424	0.459	0.420	0.490	0.823	0.561	0.421	0.423
ETM2	96	0.222	<u>0.244</u>	0.250	0.302	0.264	0.256	0.287	0.453	0.339	0.260	0.245
	192	0.256	<u>0.285</u>	0.288	0.376	0.309	0.296	0.328	0.563	0.340	0.303	0.291
	336	0.283	<u>0.322</u>	0.322	0.438	0.348	0.329	0.366	0.887	0.372	0.342	0.343
	720	0.347	<u>0.377</u>	0.380	0.482	0.407	0.385	0.415	1.388	0.419	0.421	0.399
Traffic	96	0.257	0.236	<u>0.242</u>	0.332	0.268	0.249	0.366	0.391	0.388	0.282	0.253
	192	0.310	0.241	<u>0.253</u>	0.342	0.276	0.256	0.373	0.379	0.382	0.287	0.258
	336	0.320	0.250	<u>0.261</u>	0.345	0.283	0.264	0.383	0.420	0.337	0.296	0.263
	720	0.335	<u>0.283</u>	0.287	0.357	0.302	0.286	0.382	0.472	0.408	0.315	0.282
IL1	24	0.579	0.707	<u>0.694</u>	1.309	0.883	0.754	1.260	1.449	1.182	1.081	0.823
	36	0.680	<u>0.712</u>	0.722	1.330	0.870	0.870	1.080	1.463	1.038	0.963	0.835
	48	0.710	<u>0.721</u>	0.725	1.326	0.815	0.815	1.078	1.542	1.145	1.024	0.818
	60	0.768	<u>0.737</u>	0.715	1.384	0.788	0.788	1.157	1.543	1.114	1.096	0.839

B.2 Additional Experimental Results

We evaluate StoxLSTM's CRPS across multiple datasets and prediction horizons in long-term forecasting tasks. For point prediction models, MAE and CRPS results coincide. We also assess CRPS for all baseline models. The results in Table 5 demonstrate that StoxLSTM achieves the lowest CRPS on most datasets, with xLSTM-Mixer ranking second. For instance, on the Solar dataset, StoxLSTM attains an average CRPS of 0.2135, which is **34.0%** lower than the

0.3238 average CRPS of xLSTM-Mixer. Similarly, on the ETTm2 dataset, StoxLSTM achieves an average CRPS of 0.277, outperforming xLSTM-Mixer's 0.307 by **9.8%**. These results indicate that StoxLSTM provides more accurate probabilistic forecasts across diverse datasets.

References

- [1] D. Salinas, V. Flunkert, J. Gasthaus, and T. Januschowski, “DeepAR: Probabilistic forecasting with autoregressive recurrent networks,” *International Journal of Forecasting*, vol. 36, no. 3, pp. 1181–1191, Jul. 2020. [Online]. Available: <https://www.sciencedirect.com/science/article/pii/S0169207019301888>
- [2] A. Ma, D. Luo, and M. Sha, “Mmfnet: Multi-scale frequency masking neural network for multivariate time series forecasting,” *CoRR*, vol. abs/2410.02070, 2024. [Online]. Available: <https://doi.org/10.48550/arXiv.2410.02070>
- [3] Z. Zhang, J. Wang, Y. Xia, D. Wei, and Y. Niu, “Solar-mixer: An efficient end-to-end model for long-sequence photovoltaic power generation time series forecasting,” *IEEE Transactions on Sustainable Energy*, vol. 14, no. 4, pp. 1979–1991, 2023.
- [4] N. Uremović, M. Bizjak, P. Sukić, G. Štumberger, B. Žalik, and N. Lukac, “A new framework for multivariate time series forecasting in energy management system,” *IEEE Transactions on Smart Grid*, vol. 14, no. 4, pp. 2934–2947, 2023.
- [5] H. Bi, M. Kyryliuk, Z. Wang, C. Meo, Y. Wang, R. Imhoff, R. Uijlenhoet, and J. Dauwels, “Nowcasting of extreme precipitation using deep generative models,” in *ICASSP 2023 - 2023 IEEE International Conference on Acoustics, Speech and Signal Processing (ICASSP)*, 2023, pp. 1–5.
- [6] V. P, T. Priya B, A. Rithiga B, and B. R, “Parkinson disease detection based on speech using various machine learning models and deep learning models,” in *2021 International Conference on System, Computation, Automation and Networking (ICSCAN)*, 2021, pp. 1–6.
- [7] J. L. Elman, “Finding structure in time,” *Cognitive Science*, vol. 14, no. 2, pp. 179–211, 1990.
- [8] S. Hochreiter and J. Schmidhuber, “Long short-term memory,” *Neural Computation*, vol. 9, no. 8, pp. 1735–1780, 1997.
- [9] K. Cho, B. van Merriënboer, C. Gulcehre, D. Bahdanau, F. Bougares, H. Schwenk, and Y. Bengio, “Learning phrase representations using rnn encoder-decoder for statistical machine translation,” 2014. [Online]. Available: <https://arxiv.org/abs/1406.1078>
- [10] J. Chung, C. Gulcehre, K. Cho, and Y. Bengio, “Empirical Evaluation of Gated Recurrent Neural Networks on Sequence Modeling,” Dec. 2014, arXiv:1412.3555 [cs]. [Online]. Available: <http://arxiv.org/abs/1412.3555>
- [11] S. S. Rangapuram, M. W. Seeger, J. Gasthaus, L. Stella, Y. Wang, and T. Januschowski, “Deep State Space Models for Time Series Forecasting,” in *Advances in Neural Information Processing Systems*, vol. 31. Curran Associates, Inc., 2018.
- [12] S. Chang, Y. Zhang, W. Han, M. Yu, X. Guo, W. Tan, X. Cui, M. Witbrock, M. Hasegawa-Johnson, and T. S. Huang, “Dilated Recurrent Neural Networks,” Nov. 2017, arXiv:1710.02224 [cs]. [Online]. Available: <http://arxiv.org/abs/1710.02224>
- [13] H. Zhou, S. Zhang, J. Peng, S. Zhang, J. Li, H. Xiong, and W. Zhang, “Informer: Beyond Efficient Transformer for Long Sequence Time-Series Forecasting,” *Proceedings of the AAAI Conference on Artificial Intelligence*, vol. 35, no. 12, pp. 11106–11115, May 2021, number: 12. [Online]. Available: <https://ojs.aaai.org/index.php/AAAI/article/view/17325>
- [14] M. Beck, K. Pöppel, M. Spanring, A. Auer, O. Prudnikova, M. Kopp, G. Klambauer, J. Brandstetter, and S. Hochreiter, “xlstm: Extended long short-term memory,” *CoRR*, vol. abs/2405.04517, 2024. [Online]. Available: <https://doi.org/10.48550/arXiv.2405.04517>
- [15] Y. Kong, Z. Wang, Y. Nie, T. Zhou, S. Zohren, Y. Liang, P. Sun, and Q. Wen, “Unlocking the power of LSTM for long term time series forecasting,” *CoRR*, vol. abs/2408.10006, 2024. [Online]. Available: <https://doi.org/10.48550/arXiv.2408.10006>
- [16] M. Kraus, F. Divo, D. S. Dhami, and K. Kersting, “xlstm-mixer: Multivariate time series forecasting by mixing via scalar memories,” *CoRR*, vol. abs/2410.16928, 2024. [Online]. Available: <https://doi.org/10.48550/arXiv.2410.16928>
- [17] M. Alharthi and A. Mahmood, “xlstmtime : Long-term time series forecasting with xlstm,” *CoRR*, vol. abs/2407.10240, 2024. [Online]. Available: <https://doi.org/10.48550/arXiv.2407.10240>

- [18] J. Durbin and S. J. Koopman, *Time Series Analysis by State Space Methods*. Oxford University Press, May 2012. [Online]. Available: <https://academic.oup.com/book/16563>
- [19] L. Girin, S. Leglaive, X. Bie, J. Diard, T. Hueber, and X. Alameda-Pineda, *Dynamical Variational Autoencoders: A Comprehensive Review*. Foundations and Trends® in Machine Learning, 2021, vol. 15.
- [20] M. Fraccaro, S. r. K. Sønderby, U. Paquet, and O. Winther, “Sequential Neural Models with Stochastic Layers,” in *Advances in Neural Information Processing Systems*, D. Lee, M. Sugiyama, U. Luxburg, I. Guyon, and R. Garnett, Eds., vol. 29. Curran Associates, Inc., 2016. [Online]. Available: https://proceedings.neurips.cc/paper_files/paper/2016/file/208e43f0e45c4c78cafadb83d2888cb6-Paper.pdf
- [21] J. Ye, C. Zhou, X. Zhou, Y. Huang, and C. Zhao, “Cvacl-ma: Comprehensive variate analysis and collaborative learning with multi-adapter for multivariate time series forecasting,” *Pattern Recognition*, vol. 169, p. 111936, 2026. [Online]. Available: <https://www.sciencedirect.com/science/article/pii/S0031320325005965>
- [22] G. Tan, Y. Wang, Z. Xiao, D. He, and G. Sa, “From a multi-period perspective: A periodic dynamics forecasting network for multivariate time series forecasting,” *Pattern Recognition*, vol. 167, p. 111760, 2025. [Online]. Available: <https://www.sciencedirect.com/science/article/pii/S0031320325004200>
- [23] A. Vaswani, N. Shazeer, N. Parmar, J. Uszkoreit, L. Jones, A. N. Gomez, L. Kaiser, and I. Polosukhin, “Attention is all you need,” in *Advances in Neural Information Processing Systems 30: Annual Conference on Neural Information Processing Systems 2017, December 4-9, 2017, Long Beach, CA, USA*, I. Guyon, U. von Luxburg, S. Bengio, H. M. Wallach, R. Fergus, S. V. N. Vishwanathan, and R. Garnett, Eds., 2017, pp. 5998–6008. [Online]. Available: <https://proceedings.neurips.cc/paper/2017/hash/3f5ee243547dee91fbd053c1c4a845aa-Abstract.html>
- [24] H. Wu, J. Xu, J. Wang, and M. Long, “Autoformer: Decomposition transformers with auto-correlation for long-term series forecasting,” in *Advances in Neural Information Processing Systems 34: Annual Conference on Neural Information Processing Systems 2021, NeurIPS 2021, December 6-14, 2021, virtual*, M. Ranzato, A. Beygelzimer, Y. N. Dauphin, P. Liang, and J. W. Vaughan, Eds., 2021, pp. 22 419–22 430. [Online]. Available: <https://proceedings.neurips.cc/paper/2021/hash/bcc0d400288793e8bcd7c19a8ac0c2b-Abstract.html>
- [25] Y. Zhang and J. Yan, “Crossformer: Transformer utilizing cross-dimension dependency for multivariate time series forecasting,” in *The Eleventh International Conference on Learning Representations, ICLR 2023, Kigali, Rwanda, May 1-5, 2023*. OpenReview.net, 2023. [Online]. Available: <https://openreview.net/forum?id=vSVLM2j9eie>
- [26] T. Zhou, Z. Ma, Q. Wen, X. Wang, L. Sun, and R. Jin, “FEDformer: Frequency Enhanced Decomposed Transformer for Long-term Series Forecasting,” in *Proceedings of the 39th International Conference on Machine Learning*. PMLR, Jun. 2022, pp. 27 268–27 286, iSSN: 2640-3498. [Online]. Available: <https://proceedings.mlr.press/v162/zhou22g.html>
- [27] A. Zeng, M. Chen, L. Zhang, and Q. Xu, “Are transformers effective for time series forecasting?” in *Thirty-Seventh AAAI Conference on Artificial Intelligence, AAAI 2023, Thirty-Fifth Conference on Innovative Applications of Artificial Intelligence, IAAI 2023, Thirteenth Symposium on Educational Advances in Artificial Intelligence, EAAI 2023, Washington, DC, USA, February 7-14, 2023*, B. Williams, Y. Chen, and J. Neville, Eds. AAAI Press, 2023, pp. 11 121–11 128. [Online]. Available: <https://doi.org/10.1609/aaai.v37i9.26317>
- [28] S. Wang, H. Wu, X. Shi, T. Hu, H. Luo, L. Ma, J. Y. Zhang, and J. Zhou, “Timemixer: Decomposable multiscale mixing for time series forecasting,” in *The Twelfth International Conference on Learning Representations, ICLR 2024, Vienna, Austria, May 7-11, 2024*. OpenReview.net, 2024. [Online]. Available: <https://openreview.net/forum?id=7oLshfEIC2>
- [29] S. Wang, J. Li, X. Shi, Z. Ye, B. Mo, W. Lin, S. Ju, Z. Chu, and M. Jin, “TimeMixer++: A General Time Series Pattern Machine for Universal Predictive Analysis,” Oct. 2024, arXiv:2410.16032 [cs]. [Online]. Available: <http://arxiv.org/abs/2410.16032>
- [30] Z. Li, S. Qi, Y. Li, and Z. Xu, “Revisiting Long-term Time Series Forecasting: An Investigation on Linear Mapping,” May 2023, arXiv:2305.10721 [cs]. [Online]. Available: <http://arxiv.org/abs/2305.10721>
- [31] Y. Liu, T. Hu, H. Zhang, H. Wu, S. Wang, L. Ma, and M. Long, “itransformer: Inverted transformers are effective for time series forecasting,” in *The Twelfth International Conference on Learning Representations, ICLR 2024, Vienna, Austria, May 7-11, 2024*. OpenReview.net, 2024. [Online]. Available: <https://openreview.net/forum?id=JePfAI8fah>
- [32] Y. Nie, N. H. Nguyen, P. Sinthong, and J. Kalagnanam, “A time series is worth 64 words: Long-term forecasting with transformers,” in *The Eleventh International Conference on Learning Representations, ICLR 2023, Kigali, Rwanda, May 1-5, 2023*. OpenReview.net, 2023. [Online]. Available: <https://openreview.net/forum?id=Jbdc0vTOcol>

- [33] G. E. P. Box and G. M. Jenkins, “Some Recent Advances in Forecasting and Control,” *Journal of the Royal Statistical Society. Series C (Applied Statistics)*, vol. 17, no. 2, pp. 91–109, 1968, publisher: [Royal Statistical Society, Oxford University Press]. [Online]. Available: <https://www.jstor.org/stable/2985674>
- [34] H. Lütkepohl, *New Introduction to Multiple Time Series Analysis* | SpringerLink. Springer Science & Business Media, 2005.
- [35] I. Goodfellow, J. Pouget-Abadie, M. Mirza, B. Xu, D. Warde-Farley, S. Ozair, A. Courville, and Y. Bengio, “Generative adversarial networks,” *Commun. ACM*, vol. 63, no. 11, p. 139–144, Oct. 2020. [Online]. Available: <https://doi.org/10.1145/3422622>
- [36] J. Yoon, D. Jarrett, and M. van der Schaar, “Time-series Generative Adversarial Networks,” in *Advances in Neural Information Processing Systems*, H. Wallach, H. Larochelle, A. Beygelzimer, F. d. Alché-Buc, E. Fox, and R. Garnett, Eds., vol. 32. Curran Associates, Inc., 2019. [Online]. Available: https://proceedings.neurips.cc/paper_files/paper/2019/file/c9efe5f26cd17ba6216bbe2a7d26d490-Paper.pdf
- [37] J. Ho, A. Jain, and P. Abbeel, “Denoising Diffusion Probabilistic Models,” in *Advances in Neural Information Processing Systems*, H. Larochelle, M. Ranzato, R. Hadsell, M. F. Balcan, and H. Lin, Eds., vol. 33. Curran Associates, Inc., 2020, pp. 6840–6851. [Online]. Available: https://proceedings.neurips.cc/paper_files/paper/2020/file/4c5bcfec8584af0d967f1ab10179ca4b-Paper.pdf
- [38] K. Rasul, C. Seward, I. Schuster, and R. Vollgraf, “Autoregressive denoising diffusion models for multivariate probabilistic time series forecasting,” in *Proceedings of the 38th International Conference on Machine Learning*, ser. Proceedings of Machine Learning Research, M. Meila and T. Zhang, Eds., vol. 139. PMLR, 18–24 Jul 2021, pp. 8857–8868. [Online]. Available: <https://proceedings.mlr.press/v139/rasul21a.html>
- [39] B. Tang and D. S. Matteson, “Probabilistic Transformer For Time Series Analysis,” in *Advances in Neural Information Processing Systems 34: Annual Conference on Neural Information Processing Systems 2021, NeurIPS 2021, December 6-14, 2021, virtual*, M. Ranzato, A. Beygelzimer, Y. N. Dauphin, P. Liang, and J. W. Vaughan, Eds., 2021, pp. 23 592–23 608. [Online]. Available: <https://proceedings.neurips.cc/paper/2021/hash/c68bd9055776bf38d8fc43c0ed283678-Abstract.html>
- [40] D. P. Kingma and M. Welling, “Auto-encoding variational bayes,” *CoRR*, vol. abs/1312.6114, 2013. [Online]. Available: <https://api.semanticscholar.org/CorpusID:216078090>
- [41] J. Bayer and C. Osendorfer, “Learning Stochastic Recurrent Networks,” Mar. 2015, arXiv:1411.7610 [stat]. [Online]. Available: <http://arxiv.org/abs/1411.7610>
- [42] Z. Wang, Y. Li, Z. Gong, and M. Zhu, “Mspf-trans: A generative transformer for multistep probabilistic forecasting of radar pulse repetition interval sequences,” *IEEE Transactions on Aerospace and Electronic Systems*, vol. 61, no. 2, pp. 1725–1741, 2025.
- [43] G. Lai, W.-C. Chang, Y. Yang, and H. Liu, “Modeling long- and short-term temporal patterns with deep neural networks,” in *The 41st International ACM SIGIR Conference on Research & Development in Information Retrieval*, ser. SIGIR ’18. New York, NY, USA: Association for Computing Machinery, 2018, p. 95–104. [Online]. Available: <https://doi.org/10.1145/3209978.3210006>
- [44] L. Liu, H. Jiang, P. He, W. Chen, X. Liu, J. Gao, and J. Han, “On the Variance of the Adaptive Learning Rate and Beyond,” Oct. 2021, arXiv:1908.03265 [cs]. [Online]. Available: <http://arxiv.org/abs/1908.03265>